W-Band Waveguide Bandpass Filters Fabricated by Micro Laser Sintering

Milan Salek, Xiaobang Shang, *Member, IEEE*, Robert C. Roberts, *Member, IEEE*, Michael J. Lancaster, *Senior Member, IEEE*, Falko Boettcher, Daniel Weber, and Thomas Starke

***Abstract*—This brief presents a fifth-order W-band waveguide bandpass filter with a Chebyshev response, operating at center frequency of 90 GHz and having fractional bandwidth of 11%. The filter is fabricated by micro laser sintering process which is a powder bed based additive manufacturing technology. Use of this technology allows the filter to be made accurately with high resolution and good surface quality in one piece. This results in better performance in term of insertion loss and reproducibility. For the purpose of comparison, two similar filters are presented in this brief with the same structure and specification, one made from stainless steel and the other made from stainless steel coated with copper. Both filters are tested and have excellent agreement between measurements and simulations.**

***Index Terms*—3-D printing, micro laser sintering process, stereolithography, W-band, waveguide bandpass filter.**

I. Introduction

USING additive manufacturing technologies to fabricate microwave components has become of interest in recent years. Both metallic and non-metallic materials are used in additive manufacturing fabrication processes, but non-metallic materials generally need to be coated with a conductive layer using a surface metallization process to achieve a good electrical conductivity.

Using additive technologies allows components with complex structure to be fabricated at low cost with high accuracy. Many different types of additive manufacturing technologies are available such as stereolithography apparatus (SLA), fused deposition modelling (FDM) and selective laser sintering (SLS) [1]. Fabrication of microwave filters operating at both low and high frequencies (0.5 GHz to 100 GHz) using the stereolithography-based 3-D printing technique is well proven to work with good results as shown in [1]–[11]. Other microwave components produced by stereolithography-based 3-D printing are antennas with examples reported in [12]–[16].

Stereolithography-based 3-D printing makes use of photodefinable plastic materials; so printed filters must be subsequently coated with conductive materials using surface metallization process. This results in an increase in complexity of the fabrication process and cost. However, using the micro laser sintering process allows metallic materials to be used directly. Using a metallic fabrication process increases the strength of components, as well as insuring wider working temperature range and better thermal expansion properties.

This brief describes a W-band waveguide bandpass filter, which is fabricated by micro laser sintering, also known as selective laser sintering or selective laser melting. Using this technique allows the filter to be manufactured with high accuracy, high resolution and good surface quality.

The filter reported here operates at center frequency of 90 GHz with bandwidth of 10 GHz, and to the best of author's knowledge this is the highest frequency filter fabricated by micro laser sintering process. The waveguide bandpass filter design is reasonably conventional, using coupling matrix theory to design a filter based on five rectangular resonators which are coupled using inductive irises [17], [18]. In addition to the waveguide filter, the standard UG387/U flange was included in the fabrication process enabling accurate connection to measurement system.

There are many different types of conductive powder materials that are commonly used in the micro laser sintering process such as stainless steel, molybdenum and tungsten. Stainless steel used in fabrication process of both filters with one being coated with copper to compare insertion loss.

II. Bandpass Filter Design

The filter is constructed with five coupled rectangular resonators operating in the TE_{101} mode. The couplings between the resonators as well as input/ output coupling are realized using inductive irises. The filter is specified in terms of the Chebyshev bandpass response with center frequency of

Manuscript received February 12, 2018; revised March 22, 2018; accepted April 5, 2018. Date of publication April 10, 2018; date of current version December 20, 2018. This work was supported in part by the U.K. Engineering and Physical Science Research Council under Contract EP/M016269/1 and in part by the 3-D Micro Print Gmbh in Germany and Additive Microfabrication Laboratory, University of Hong Kong. This brief was recommended by Associate Editor I. W. H. Ho. *(Corresponding author: Milan Salek.)*

M. Salek and M. J. Lancaster are with the Department of Electronic, Electrical and Systems Engineering, University of Birmingham, Birmingham B15 2TT, U.K. (e-mail: mxs1149@bham.ac.uk; m.j.lancaster@bham.ac.uk).

X. Shang was with the Department of Electronic, Electrical and Systems Engineering, University of Birmingham, Birmingham B15 2TT, U.K. He is now with the Engineering, Materials and Electrical Science Department, National Physical Laboratory, Middlesex TW11 0LW, U.K. (e-mail: xiaobang.shang@npl.co.uk).

R. C. Roberts is with the Department of Computer Science, University of Hong Kong, Hong Kong (e-mail: rcr8@hku.hk).

F. Boettcher and T. Starke are with 3-D Micro Print Gmbh, 09126 Chemnitz, Germany (e-mail: falko.boettcher@3dmicroprint.com; thomas.starke@3dmicroprint.com).

D. Weber was with the 3-D Micro Print Gmbh, 09126 Chemnitz, Germany. He is now with Freeman Technology, Tewkesbury GL20 8DN, U.K. (e-mail: engineering.daniel.weber@gmail.com).

Color versions of one or more of the figures in this paper are available online at http://ieeexplore.ieee.org.

Digital Object Identifier 10.1109/TCSII.2018.2824898

90 GHz, bandwidth of 10 GHz (fractional bandwidth of 11%) and return loss of 20 dB over the passband. Using coupling matrix theory [17], the filter specification is translated into coupling matrix elements, which are then translated into physical dimensions according to the procedure in [17] and [18].

A coupling routing diagram of the filter can be seen in Fig. 1 (a). The un-normalized non-zero coupling coefficients between resonators are $M_{12} = M_{45} = 0.0961$, $M_{23} = M_{34} = 0.0706$ and the external quality factor of the first (Q_{e1}) and the last (Q_{en}) resonators are calculated to be $Q_{e1} = Q_{en} = 8.76$ [17], [18].

The physical dimensions which correspond to the coupling and Q values are found by the standard technique. Looking at Fig. 1 (b), it can be seen that coupling between resonators is realized by the width of irises, which are denoted by $D_1 = D_4$ and $D_2 = D_3$ and set by coupling coefficients $M_{12} = M_{45}$ and $M_{23} = M_{34}$ respectively. The input/ output coupling is realized by adjusting the width of the iris denoted by E, which is set by external quality factors $Q_{e1} = Q_{en}$. Simulations and final optimization of the filter are carried out in CST Microwave Studio [19] to get the frequency response close to the ideal.

Fig. 1 (c) illustrates the external design of the W-band waveguide bandpass filter, along with its external dimensions in millimeters. Fig. 1 (d) shows a cross section view of the filter with the resonators and all internal couplings between resonators shown. The screw holes, alignment pin holes and precision alignment pin holes are included in both input and output UG387/U waveguide flanges. The filter and flange are designed in the hexagonal shape in order to facilitate fabrication by the micro laser sintering process.

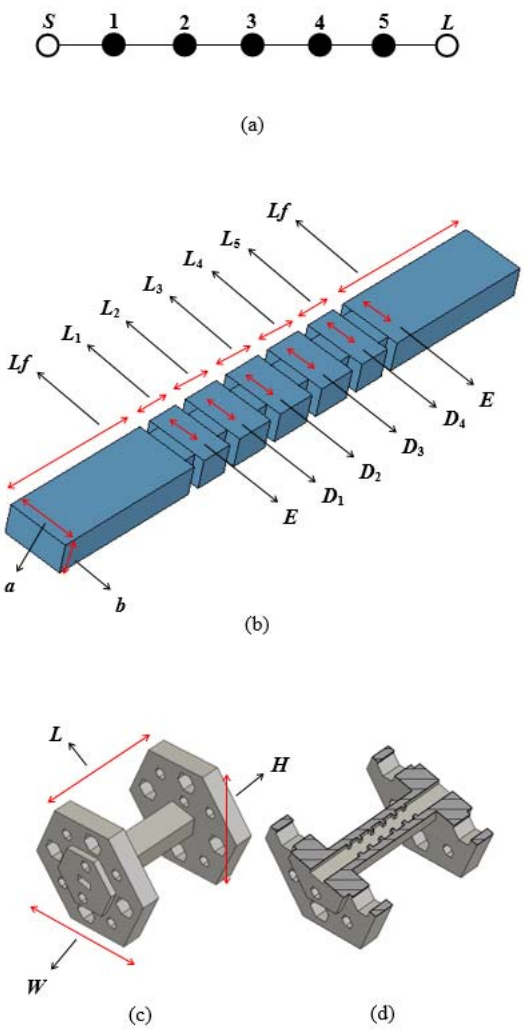

Fig. 1. Illustration of the fifth-order waveguide bandpass filter. (a) Coupling routing diagram of the filter. (b) Internal structure of the filter showing internal dimensions. The dimensions in millimeter are: $Lf = 6.48$, $L_1 = L_5 = 1.317$, $L_2 = L_4 = 1.582$, $L_3 = 1.636$, $E = 1.7$, $D_1 = D_4 = 1.374$, $D_2 = D_3 = 1.291$, $a = 2.54$ and $b = 1.27$. (c) Completed filter, showing external dimensions. The dimensions in millimeter are: $L = 21.4$, $H = 19.05$ and $W = 22$. (d) A cross section view of the filter showing internal couplings between resonators.

III. Micro Laser Sintering Fabrication Process

Micro laser sintering is an additive manufacturing process, which is by far the most accurate sintering fabrication process to 3D print solid metal structures. Using the micro laser sintering process enables parts with complex 3D micro structures to be produced at reasonable costs, where conventional additive manufacturing processes reach their limits. In the process the model structure is divided into layers, and each layer is printed by applying a thin layer of metal powder to a build platform and then, using a laser beam, the powder is selectively fused according to the required layer structure. Once a layer is constructed, the building platform is lowered, and next layer will be constructed with same process as in previous layers. The process continues until all layers are constructed on top of each other according to 3D model structure [20]. The accuracy of micro laser sintering makes this fabrication process attractive for fabricating high frequency waveguide filters, as it enables the production of small filters with complex structures and high strength.

Two similar filters with the same structure and specification were made to compare insertion loss. Both filters made from stainless steel with one being coated with copper. The filters were fabricated by 3D Micro Print Gmbh [20], using their micro laser sintering process in an inert argon atmosphere. The laser source was an IR fiber laser with a 50 W laser average power. The laser spot diameter is focused down to 30 μm and was operated in continuous wave mode. The filters are made from stainless steel powder material with one being coated with a 5μm thick copper layer by electroplating the surface. The type of stainless steel was 1.4542 (17-4PH) according to ASTM 564, which is a chromium nickel copper alloyed stainless steel, containing 17% chromium, 4% nickel, 4% copper and 0.3% niobium. The powder particle sizes were smaller than d_{80} 5μm and had electrical conductivity of 1.25×10^7 S/m. The thickness of each layer in the process was set at 5μm. The print took about 16 hours, but this could be considerably reduced by optimizing the build process further.

Fig. 2 (a) shows photograph of the filter on the support structure after fabrication. Fig. 2 (b) provides a photograph of the fabricated filter made from Stainless Steel and Fig. 2 (c) shows the fabricated filter made from stainless steel after being

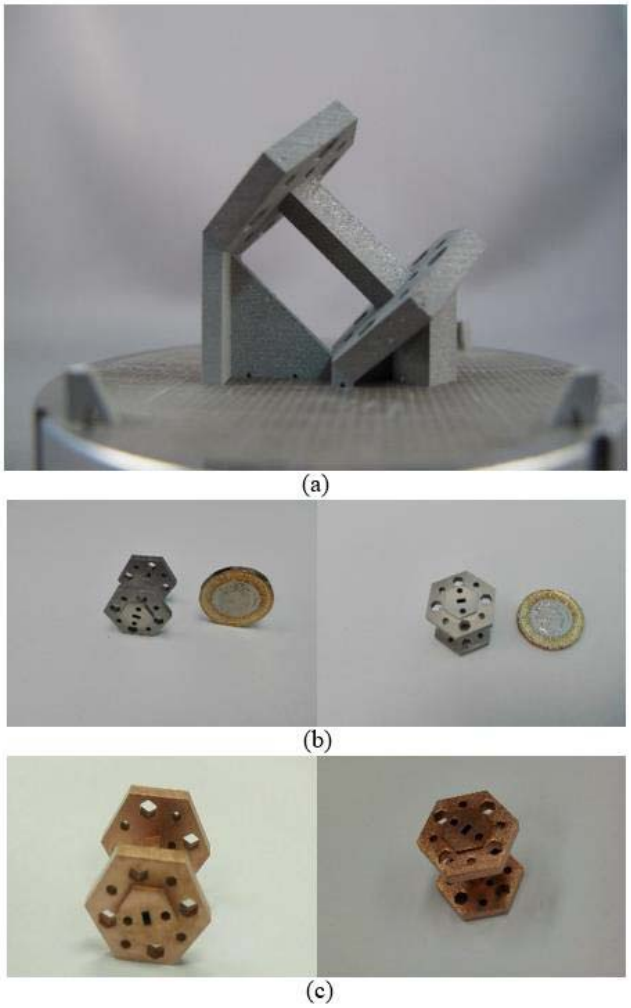

Fig. 2. Photograph of the fabricated W-band waveguide bandpass filter. (a) Filter on support structure after fabrication process. (b) Fabricated filter made from stainless steel. (c) Fabricated filter made from stainless steel, coated with copper.

electroplated with 5μm thick copper layer with electrical conductivity of 5.96×10^7 S/m.

IV. Measurement and Discussion

The *S*-parameter measurements of both filters are performed on Keysight E8361C PNA network analyzer. Fig. 3 shows photograph of the measurement setup. Here the filter is placed between two waveguide flanges of the network analyzer, aligned using four precision alignment pins of the waveguide flanges and tightened using four screws on each side. Fig. 4 and Fig. 5 show the measured and simulated results of both W-band waveguide bandpass filters, where the measured results are denoted with solid lines and simulated results with dashed lines. Looking at the stainless steel filter in Fig. 4 (a), it can be seen that the measured center frequency, shifts down by 1.66 GHz and a minimum return loss of 24.41 dB across the whole passband. Looking at the copper coated filter in Fig. 5 (a), it can be observed that the frequency shift is only 0.9 GHz and a minimum return loss of 26.56 dB across the whole passband. The lower return loss of 15.2 dB at 84.6 GHz

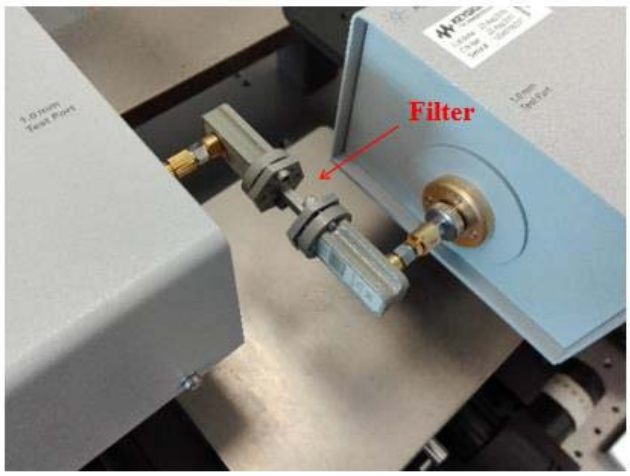

Fig. 3. Photograph of the measurement setup with the filter being placed between two waveguide flanges of the network analyzer.

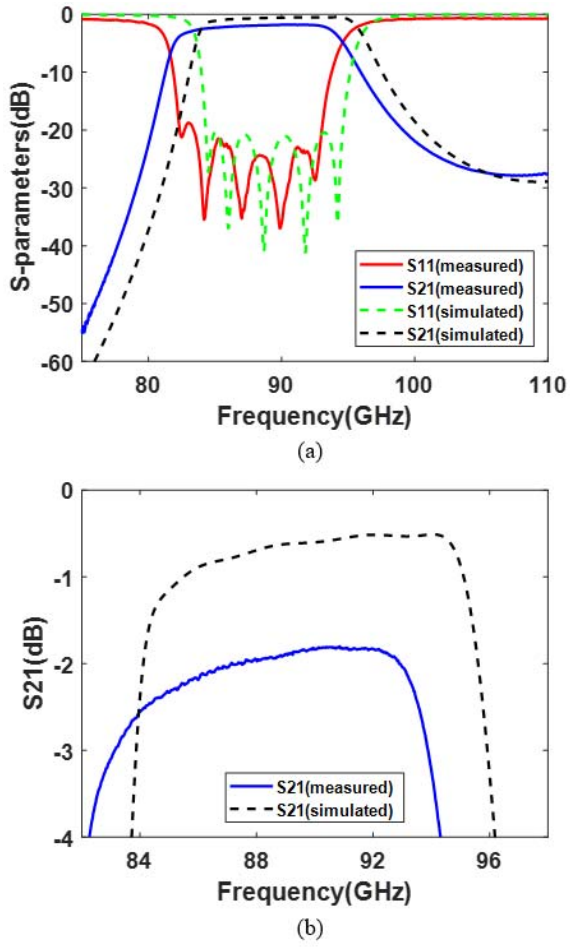

Fig. 4. Measured and simulated results of the W-band waveguide bandpass filter made from stainless steel. (a) Measured and simulated results over the whole W-band. (b) Expanded view of S_{21} over passband.

in Fig. 5 (a) is caused by slight deviation of the cavity sizes from the design and can be improved by tuning filter. To be clear, there has been no tuning of the filters and these excellent responses show the high quality of the 3D printing.

TABLE I
COMPARISON WITH OTHER WAVEGUIDE BANDPASS FILTERS

f_c (GHz)	FBW	IL (dB)	RL (dB)	Manufacturing techniques	f_c *offset*	*Reference*
107.2	6.34%	0.95	>11	SLA	7.2%	[1]
100	4%	0.5~0.8	>15	Laser micromachining	0%	[10]
87.5	11.5%	0.3~0.5	>18	SLA	2.78%	[10]
88.47	9.7%	0.97~1.1	>15	SU-8 process	1.7%	[21]
102	5%	1.2	>10	SU-8 process	2%	[22]
100	10%	0.6	>18	CNC milling	0%	[23]
92.6	4.53%	0.5	>14	CNC milling	0.02%	[24]
92.45	4.83%	1.1~1.3	>10	DRIE	1.86%	[25]
95	3.68%	3.49	>18	Hot embossing	0.52%	[26]
75.5	5.3%	8	>8	SLM	2.72%	[27]
88.34	12.1%	1.94	>18	MLS	1.84%	T.W. (stainless steel)
89.1	11.07%	1	>15	MLS	1%	T.W. (copper coted)

f_c: center frequency of the filter; FBW: fractional bandwidth; IL: passband insertion loss; RL: passband return loss; f_c offset: frequency shift; T.W.: this work.

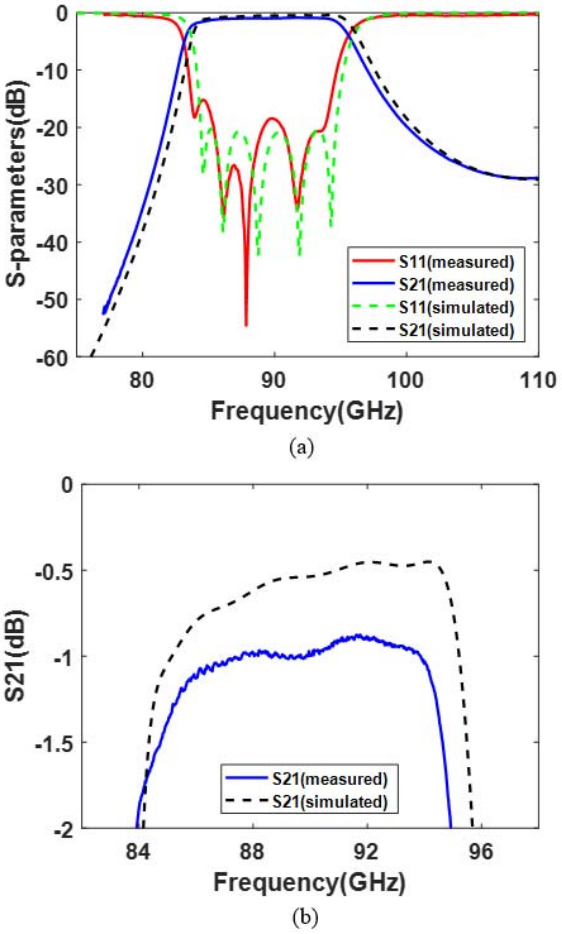

Fig. 5. Measured and simulated results of the W-band waveguide bandpass filter made from stainless steel coated with 5μm thick copper layer. (a) Measured and simulated results over the whole W-band. (b) Expanded view of S_{21} over passband.

The unwanted frequency shifts in the filters is believed to be caused by small dimensional inaccuracies, as a result of expansion in length of resonators, which could be corrected by remanufacturing. It has been found that such an expansion of dimensions is repeatable and as both filters have small frequency shift, the model could be adjusted accordingly to compensate during the remanufacturing.

Careful examination of the expanded view of S_{21} in Fig. 4 (b) shows an average insertion loss of around 1.94 dB over the passband for the measured results, which is 1.34 dB higher than the simulated results. The expanded view of S_{21} in Fig. 5 (b) shows an average insertion loss of around 1 dB over the passband for the measured results, which is 0.47 dB higher than simulated results. Note, the copper plated filter has 0.94 dB lower measured insertion loss in comparison to the filter made from stainless steel showing the advantages of the copper coating.

The typical surface roughness values of the filters measured with Mitutoyo SurfTest SV-3000 CNC surface roughness tester is about 2 μm. This reduces effective conductivity of stainless steel to 3.19×10^6 S/m and copper to 14.97×10^6 S/m. According to calculations [19] this results in additional loss of 0.456 dB for the filter that is not coated with copper and 0.453 dB for the copper coated filter, however this loss is already reflected in the CST simulated results. The loss in the waveguide jointing the filter to the flanges (0.075dB) is also included in the simulations. In addition, small misalignments during measurements also contribute to the difference in insertion loss but show up in the return loss. The 20 dB return loss contributes about 0.1 dB to the insertion loss.

The additional difference in insertion loss between simulation and measurement is probably caused by a combination of factors including the estimate of the conductivity of the stainless steel and copper which may not be as specified due to impurities, surface contaminates, or oxidation. There may be effects because of the granular nature of the surface formed from the powder as well as changes from the specified stainless steel conductivity because of the manufacturing process. Because of the high frequency and the small skin depth, the loss is highly dependent on these surface effects. A further detailed study is required here to understand these losses. The insertion loss can be improved by electroplating the surface (as we have seen), laser polishing, chemical polishing and using higher conductivity powder materials.

Table I provides a comparison of measured performance of waveguide bandpass filters that are fabricated using different types of manufacturing technique.

V. Conclusion

A metal 3D printed W-band waveguide bandpass filter fabricated by micro laser sintering process has been presented in this brief. This is the highest frequency metal 3D printed filter so far reported. Good agreement between the measured and simulated results demonstrate that micro laser sintering process can be used to fabricate filters with complex structures, that operate at high frequencies accurately. The micro laser sintering technique not only offers accuracy, but it also enables the whole structure, including flanges, to be made in a single piece. In addition, using electroplated copper demonstrates, it can improve the insertion loss of the filter considerably.

References

[1] M. D'Auria *et al.*, "3-D printed metal-pipe rectangular waveguides," *IEEE Trans. Compon. Packag. Manuf. Technol.*, vol. 5, no. 9, pp. 1339–1349, Sep. 2015.

[2] X. Shang, J. Li, C. Guo, M. J. Lancaster, and J. Xu, "3-D printed filter based on helical resonators with variable width," in *Proc. IEEE MTT-S Int. Microw. Symp. (IMS)*, 2017, pp. 1587–1590.

[3] C. Guo, J. Li, J. Xu, and H. Li, "An X-band lightweight 3-D printed slotted circular waveguide dual-mode bandpass filter," in *Proc. IEEE Int. Symp. Antennas Propag. USNC/URSI Nat. Radio Sci. Meeting*, 2017, pp. 2645–2646.

[4] L. Araujo *et al.*, "3-D printed band-pass combline filter," *Microw. Opt. Technol. Lett.*, vol. 59, no. 6, pp. 1388–1390, 2017.

[5] C. Guo, X. Shang, M. J. Lancaster, and J. Xu, "A 3-D printed lightweight X-band waveguide filter based on spherical resonators," *IEEE Microw. Wireless Compon. Lett.*, vol. 25, no. 7, pp. 442–444, Jul. 2015.

[6] C. Guo *et al.*, "A lightweight 3-D printed X-band bandpass filter based on spherical dual-mode resonators," *IEEE Microw. Wireless Compon. Lett.*, vol. 26, no. 8, pp. 568–570, Aug. 2016.

[7] C. Guo *et al.*, "Ceramic filled resin based 3D printed X-band dual-mode bandpass filter with enhanced thermal handling capability," *Electron. Lett.*, vol. 52, no. 23, pp. 1929–1931, Oct. 2016.

[8] J. Li, C. Guo, L. Mao, and J. Xu, "Compact high-Q hemispherical resonators for 3-D printed bandpass filter applications," in *Proc. IEEE MTT-S Int. Microw. Symp. (IMS)*, 2017, pp. 1591–1594.

[9] J. Li, C. Guo, J. Xu, and L. Mao, "Lightweight low-cost Ka-band 3-D printed slotted rectangular waveguide bandpass filters," in *Proc. IEEE Int. Symp. Antennas Propag. USNC/URSI Nat. Radio Sci. Meeting*, 2017, pp. 2647–2648.

[10] X. Shang *et al.*, "W-band waveguide filters fabricated by laser micromachining and 3-D printing," *IEEE Trans. Microw. Theory Techn.*, vol. 64, no. 8, pp. 2572–2580, Aug. 2016.

[11] G. Venanzoni, M. Dionigi, C. Tomassoni, D. Eleonori, and R. Sorrentino, "3D printing of X band waveguide resonators and filters," in *Proc. 32nd Gen. Assembly Sci. Symp. Int. Union Radio Sci. (URSI GASS)*, 2017, pp. 1–2.

[12] M. V. D. Vorst and J. Gumpinger, "Applicability of 3D printing techniques for compact Ku-band medium/high-gain antennas," in *Proc. 10th Eur. Conf. Antennas Propag. (EuCAP)*, 2016, pp. 1–4.

[13] F. Bongard, M. Gimersky, S. Doherty, X. Aubry, and M. Krummen, "3D-printed Ka-band waveguide array antenna for mobile SATCOM applications," in *Proc. 11th Eur. Conf. Antennas Propag. (EUCAP)*, 2017, pp. 579–583.

[14] K. F. Brakora, J. Halloran, and K. Sarabandi, "Design of 3-D monolithic MMW antennas using ceramic stereolithography," *IEEE Trans. Antennas Propag.*, vol. 55, no. 3, pp. 790–797, Mar. 2007.

[15] B. Liu, X. Gong, and W. J. Chappell, "Applications of layer-by-layer polymer stereolithography for three-dimensional high-frequency components," *IEEE Trans. Microw. Theory Techn.*, vol. 52, no. 11, pp. 2567–2575, Nov. 2004.

[16] J. S. Silva, E. B. Lima, J. R. Costa, C. A. Fernandes, and J. R. Mosig, "Tx-Rx lens-based satellite-on-the-move Ka-band antenna," *IEEE Antennas Wireless Propag. Lett.*, vol. 14, pp. 1408–1411, 2015.

[17] R. J. Cameron, C. M. Kudsia, and R. R. Mansour, *Microwave Filters for Communication Systems: Fundamentals, Design and Applications*. Hoboken, NJ, USA: Wiley, 2007.

[18] J.-S. Hong, *Microstrip Filters for RF/Microwave Applications*. Hoboken, NJ, USA: Wiley, 2011.

[19] Computer Simulated Technology. (2017). *Microwave Studio*. [Online]. Available: http//www.cst.com/

[20] *3D Micro Print Gmbh*. Accessed: Jan. 10, 2018. [Online]. Available: http://www.3dmicroprint.com/

[21] X. Shang, M. Ke, Y. Wang, and M. Lancaster, "Micromachined W-band waveguide and filter with two embedded H-plane bends," *IET Microw. Antennas Propag.*, vol. 5, no. 3, pp. 334–339, Feb. 2011.

[22] C. A. Leal-Sevillano *et al.*, "A pseudo-elliptical response filter at W-band fabricated with thick SU-8 photo-resist technology," *IEEE Microwave Wireless Compon. Lett.*, vol. 22, no. 3, pp. 105–107, Mar. 2012.

[23] C. A. Leal-Sevillano, J. R. Montejo-Garai, J. A. Ruiz-Cruz, and J. M. Rebollar, "Low-loss elliptical response filter at 100 GHz," *IEEE Microw. Wireless Compon. Lett.*, vol. 22, no. 9, pp. 459–461, Sep. 2012.

[24] X. Liao, L. Wan, Y. Zhang, and Y. Yin, "W-band low-loss bandpass filter using rectangular resonant cavities," *IET Microw. Antennas Propag.*, vol. 8, no. 15, pp. 1440–1444, Sep. 2014.

[25] Y. Li, P. L. Kirby, and J. Papapolymerou, "Silicon micromachined W-band bandpass filter using DRIE technique," in *Proc. Eur. Microw. Conf.*, 2006, pp. 1271–1273.

[26] F. Sammoura *et al.*, "A micromachined W-band iris filter," in *13th Int. Conf. Solid-State Sensors Actuators Microsyst. Dig. Tech. Papers. (TRANSDUCERS)*, 2005, pp. 1067–1070.

[27] B. Zhang and H. Zirath, "3D printed iris bandpass filters for millimetre-wave applications," *Electron. Lett.*, vol. 51, no. 22, pp. 1791–1793, Oct. 2015.